Author response to referee #1

The authors thank Anonymous referee #1 for their comments on the manuscript. We will take the comments into account when revising the manuscript. In this document we provide responses to each of the referee's comments (formatted as italics in indented paragraphs).

> *The weakness of the method is the assumption that the direction of the jet velocity does not change in course of its observation and it can lead to misinterpretation of measurements. Moreover, the data processing does not handle with uncertainties of velocity measurements that are rather large because the velocity distribution in the magnetosheath is hardly Maxwellian, especially when the jets are present. These factors result to uncertainty in a determination of the jet coordinate system and it is fully possible that the lack of divergence in front of jet discussed in the first paragraph of Discussion section is caused by these factors. A small rotation of the coordinate system probably would lead to the diverging patterns in front of the jet but it is a question whether the converging patterns at its end will persist under assumption of the constant jet velocity.*

We agree that the treatment of uncertainties is missing and that the full moments are error-prone for our analysis. Therefore, we repeated our analysis considering the velocity distribution functions (VDFs) and included error handling. We started with a closer look at the velocity distribution functions. A first glance, the 2D slices in the plane $V_X - V_Y$ shows only single maxima for THA, THD and THE, as shown in Figure 1.

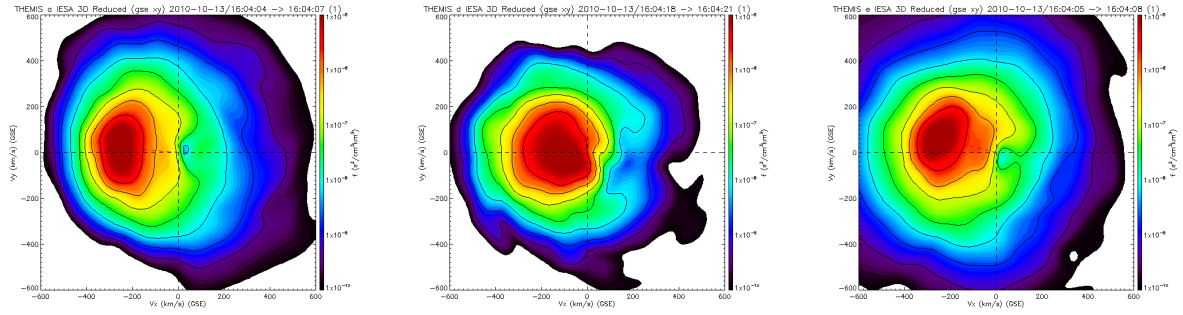

(a) THA (b) THD (c) THE

Figure 1: 2D slices of the velocity distribution around t_{max} in the $V_X - V_Y$ plane at $V_Z = 0$.

For a more detailed look, we used a similar approach as Raptis et al. [2022] and integrated the 3D distribution over two velocity axes to obtain a 1D velocity distribution along the third component. The 1D distributions along V_X, V_Y and V_Z (in GSE coordinates) at the time of maximum dynamic pressure (t_{max}) are shown in Figures 2, 3 and 4 for THA, THD and THE, respectively.

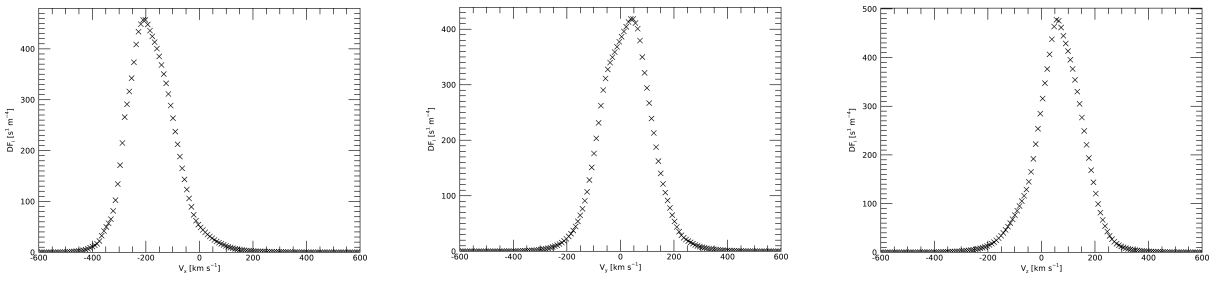

(a) THA - V_X (b) THA - V_Y (c) THA - V_Z

Figure 2: 1D distribution from integration along the other velocity axes.

Here, we were not able to see a clear bi-Maxwellian distribution for THA and THE in either of the three components [cf. Raptis et al., 2022]. Instead, we observe individual peaks, albeit with deviations from the ideal Maxwellian distribution. For THD, we clearly see two maxima in the 1D distribution along V_Y.

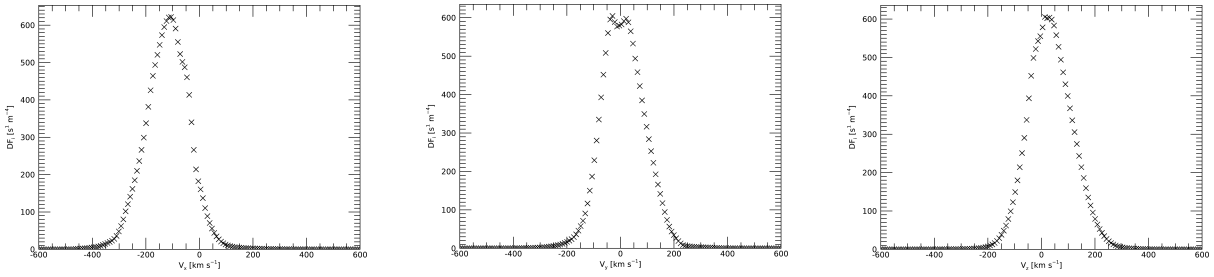

(a) THD - V_{X} (b) THD - V_{Y} (c) THD - V_{Z}

Figure 3: 1D distribution from integration along the other velocity axes.

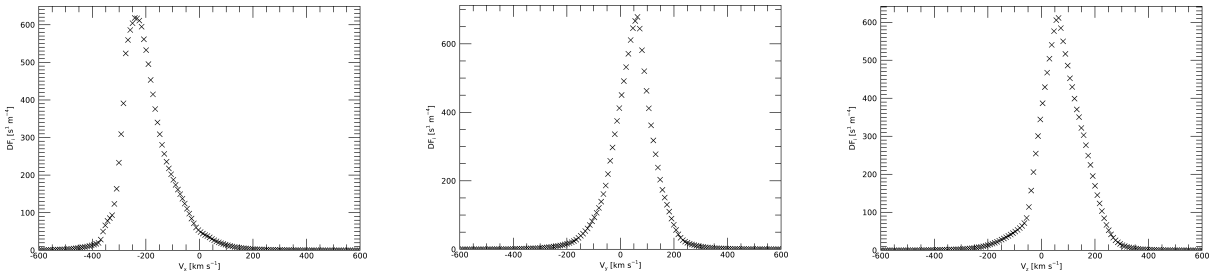

(a) THE - V_{X} (b) THE - V_{Y} (c) THE - V_{Z}

Figure 4: 1D distribution from integration along the other velocity axes.

Following the same conclusion as Raptis et al. [2022], THA and THE likely observe one plasma population. THD, which is also further away from the other two, observes two plasma populations, probably a mixture of jet and magnetosheath background plasma. Together with the lower dynamic pressure at t_{max}, this suggests that THD is closer to the edge of the jet. To be conservative, we continued our analysis using only THA and THE to determine the direction of jet propagation. Furthermore, since we see that the 1D VDFs at THA and THE deviate from ideal Maxwellians, we use the velocity at which the 1D VDF peaks in each component rather than the full plasma moments to determine the jet propagation direction. Other time steps inside the jet show similar 1D VDFs and outside the jet we observe 1D VDFs that look almost like ideal Maxwellians.

As the referee correctly stated, the direction of the jet velocity can change during the course of the observation. We therefore investigated the stability of the direction of the jet velocity. Using the updated velocity values, we calculated the polar angle Θ ($= \arccos \frac{V_z}{\sqrt{V_x^2+V_y^2+V_z^2}}$) and the azimuthal angle φ ($= \mathrm{sgn}(\mathrm{V_y}) \cdot \arccos \frac{V_x}{\sqrt{V_x^2+V_y^2}}$) of the measured velocities and plotted them over time. The results are shown in Figure 5a for all three spacecraft (for completeness, THD is also shown).

Here, we also observe a rather turbulent behavior at THD. For THA and THE, on the other hand, we see that Θ and φ are relatively constant around t_{max} (marked with black circle). To obtain a direction for the jet velocity, we determined the mean value of Θ and φ of the velocities measured by THA and THE around t_{max}. This is shown in Figure 5b. For comparison, we have also plotted the direction of THD, but we can clearly see that it deviates strongly from THA and THE. As an error, we have calculated the standard deviation and also the maximum difference in Θ and φ. To be conservative, we use the maximum difference in Θ and φ from the mean for error handling in the following analysis.

Later (in Figures 6 and 7) we show that the pattern of diverging and converging flows is not strongly dependent on the propagation direction, but is still visible when the errors are applied. In the revised version we will include the updated determination of the jet propagation direction together with the treatment of uncertainty.

Figure 2 is discussed only in terms of divergence or convergence of the flow prior to or after the jet passage but THE (that would be very close to the jet center - Figure 4) observes a relatively large velocity in the y direction. My understanding of the used coordinates is that it is the jet coordinate system and it is strange if its center moves with much larger velocity than

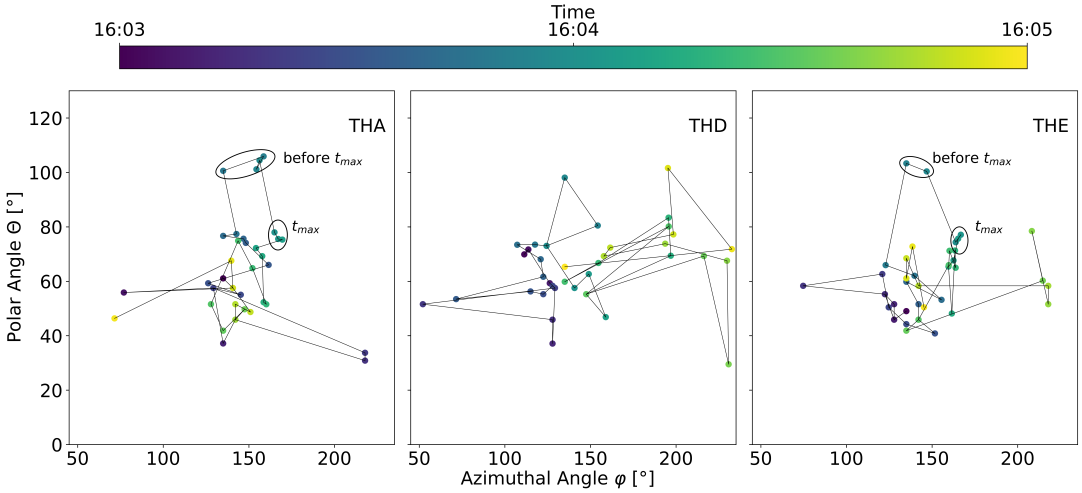

(a) Time evolution of measured velocity direction over time for THA, THD and THE in the columns from left to right. The time is color coded with darker colors corresponding to earlier times and lighter colors corresponding to later times. The polar angle Θ and the azimuthal angle φ are described in the text.

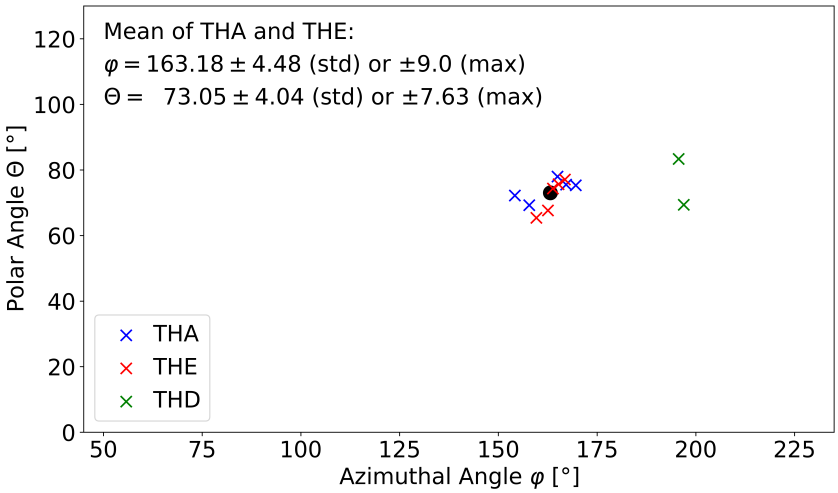

(b) Velocity direction around *t*max from THA, THD and THE in red, green and blue, respectively. The black dot corresponds to the mean value of the measurements from THA and THE.

Figure 5: Determination of propagation direction.

its surrounding. The problem of perpendicular velocities is also clear in the discussion in lines 186-189. The authors claim the largest expansion at t_max but Figure 2 shows rather contraction in the perpendicular direction at this time.

We agree that we are only discussing the flow in qualitative terms. This was done because we cannot draw any conclusions from the absolute values of the velocity. The coordinate system used in Figure 2 (in the current manuscript) shows the two axes perpendicular to the assumed direction of jet propagation. In principle, this is intended to illustrate the flow anomaly caused by the jet (namely diverging and converging flows). The greater velocity at THE indicates a greater deviation from the background flow. The larger deviation near the center is in agreement with Plaschke and Hietala [2018]. The largest expansion of the jet that we show in Figure 4 (in the current manuscript) results from our fit to the dynamic pressure measurements. We claim that the intersection between the fitting function and the dynamic pressure threshold leads to an estimate of the size of the jet. Figure 2 (in the current manuscript) should only illustrate the plasma motion around the center, and the velocities do not necessarily correlate with the size of the jet. We will revise this section as we see the need to better describe our calculations and results so that readers can more easily understand our conclusions.

The analyzed interval in all figures is +/- 12 s from the jet center (dynamic pressure peak). The jet duration is nearly 60 s in observations of all spacecraft (Figure 1). The estimated perpendicular size is about 1 Re, the distances of the spacecraft from the estimated jet center are lower than 0.4 Re (Figure 3) and it means that the analysis of the velocity components in Figures 2 and 3 are done inside the jet. However, the authors claim that the analysis is based on flows around the jet induced by the jet propagation through the magnetosheath plasma but such flows should be analyzed close to but outside of the jet.

The referee is absolutely right that the analyzed flow is inside the jet structure, and we thank the referee for pointing out the misleading description. Nevertheless, Plaschke and Hietala [2018] have shown that the evasive motion is also present inside the jet. Therefore, we should expect the same behavior with a diverging flow before and a converging flow after $t_{\max}$.
With the focus on the flow behavior within the jet, we saw the need to change our transformation to the jet coordinate system. The transformation involves only a simple rotation. We use the estimated propagation direction as the new $\mathbf{X'}$ axis and no longer subtract the background velocity. There are two reasons for this. Firstly, we only want to consider the velocity perpendicular to the propagation direction. Secondly, we do not see a bimaxwellian distribution (for THA and THE) and assume that the spacecraft observe almost exclusively the jet plasma.
We calculated $\boldsymbol{Y'}\left(=\frac{\boldsymbol{X'}\times\hat{\boldsymbol{X}}}{|\boldsymbol{X'}\times\hat{\boldsymbol{X}}|}\right)$ and $\boldsymbol{Z'}=\left(\frac{\boldsymbol{X'}\times\boldsymbol{Y'}}{|\boldsymbol{X'}\times\boldsymbol{Y'}|}\right)$ in the same way as described in the current manuscript, and we rotate the measured velocities and the positions of the spacecraft into the new coordinate system. The origin of our new coordinate system was chosen arbitrary to be at the position of the THA at $t_{\max}=[X=10.76R_{\mathrm{E}}, Y=0.34R_{\mathrm{E}}, Z=1.49R_{\mathrm{E}}]$ (in GSE coordinates). The results are shown in Figure 6 for the velocities determined from the peaks in the 1D VDFs and in Figure 7 for the velocities from the full moments for comparison. The middle rows in both figures show the resulting flow pattern when the mean jet propagation direction (see Figure 5b) is used. The bottom (top) rows of both figures show the resulting flow pattern when the errors are subtracted from (added to) the mean jet propagation direction.

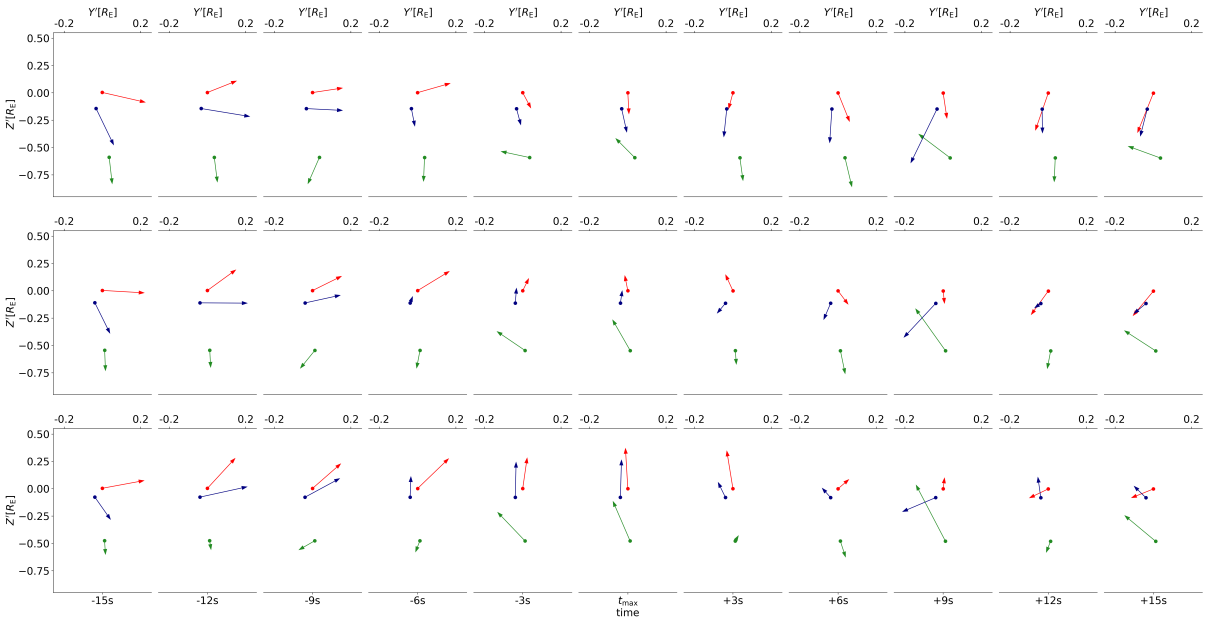

Figure 6: Flow pattern inside the jet around $t_{\max}$ with velocities from 1D-VDFs. Dots (arrows) in red, green and blue represent the position (measured velocity) of THA, THD and THE, respectively. The middle row represent the resulting flow pattern when the mean jet propagation direction is used. The bottom (top) row shows the resulting flow pattern when the errors are subtracted from (added to) the mean jet propagation direction.

We continue to consider only THA (red arrows) and THE (blue arrows), as we have already mentioned that THD observes a mixture of plasma populations. We see in all cases in the time from -15s to -6s signs of diverging velocity vectors before $t_{\max}$. Around -3s to +9s, we observe high dynamic pressure

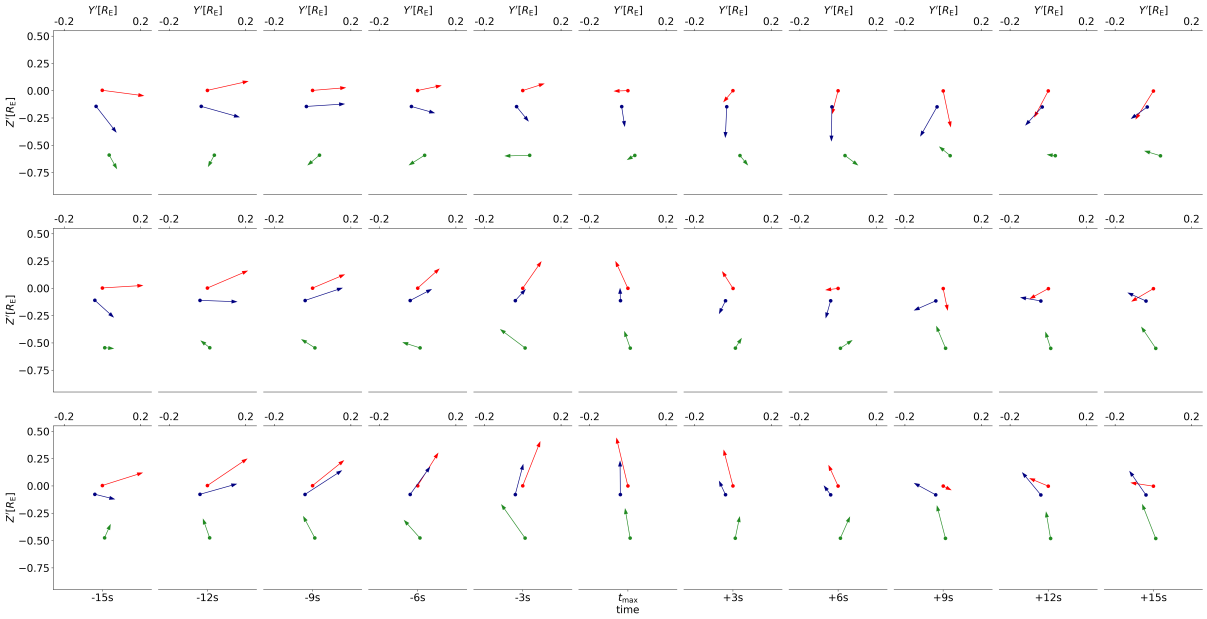

Figure 7: Flow pattern inside the jet around $t_{\max}$ with velocities from full moments. Dots (arrows) in red, green and blue represent the position (measured velocity) of THA, THD and THE, respectively. The middle rows represent the resulting flow pattern when the mean jet propagation direction is used. The bottom (top) row shows the resulting flow pattern when the errors are subtracted from (added to) the mean jet propagation direction.

(see Figure 1 in the current manuscript) and a more complex flow pattern. After $t_{\max}$ from +12s to +15s, we observe signs of the converging pattern, again in almost all cases. This should indicate the applicability of our approach even for a non-perfectly estimated propagation direction.
Furthermore, we estimated the position of the center of our jet from the diverging and converging flow at THA and THE. Figure 8 shows the temporal evolution of the center position for flow patterns determined from 1D VDFs and full moments. As we can see, the deviation of the center position is relatively small in both cases (except for errors added - top rows). In addition one can see that the center position is more stable when we use the velocities from the 1D-VDFs.
In the revised version of the manuscript we will alter the introduction and methodology accordingly and describe the new transformation together with the uncertainty treatment. We also want to point out that only two spacecraft are needed in principle to estimate the center of the jet.

> *Also two-point results given in the conclusion are not surprising, everyone expects that from the definition of a jet.*

We agree that everyone expects this result. We still see the need to show it for individual events. In addition the shape of jets is still under debate and as shown in Figure 9 there are in principle multiple possibilities for the jet shape. In all columns fits for three different times (= different intersections of the jet) are shown. The darkest color correspond to a fit at $t_{\max}$ and lighter colors correspond to later times ($t_{\max} < t_1 < t_2$). Case a) belongs to a jet which has its largest expansion around $t_{\max}$. The expansion decreases towards the front and rear parts of the jet, while the dynamic pressure stays constant. In b) one can see the opposite case with constant expansion of the jet. The dynamic pressure is highest around $t_{\max}$ and decreases toward front and rear parts. In c) both dynamic pressure and expansion are highest around $t_{\max}$ and decrease before and afterwards. While we don't expect a) to be a realistic, we can't say for sure from a single spacecraft measurement which of the cases describes the jet shape. In addition, we also wanted to point out that statistical studies on magnetosheath jets systematically underestimate the dynamic pressure as spacecraft rarely observe the center of jets.

> *Line 20 - I would suggest adding the sentence on the jet definition with corresponding reference here*

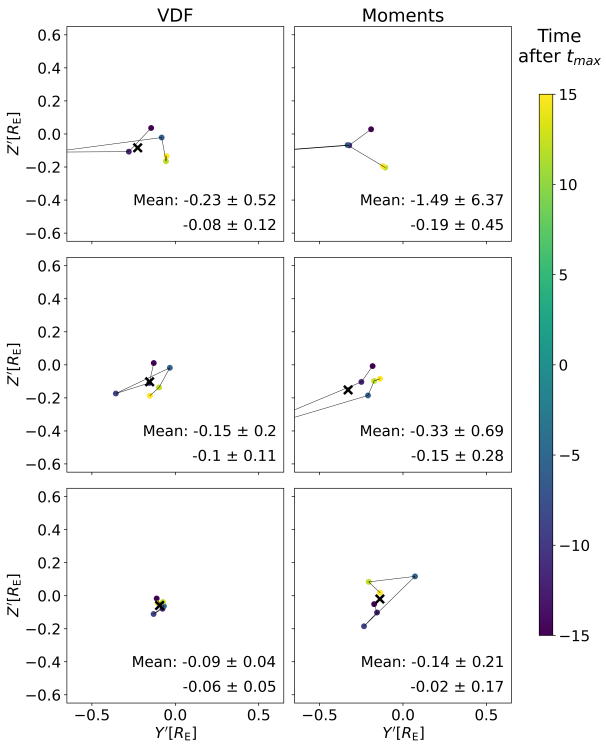

Figure 8: Time evolution of center position from the flow patterns with velocities from the 1D-VDFs (left column) and from the full moments (right column). The middle row represent the results when the mean jet propagation direction is used. The bottom (top) row shows the results when the errors are subtracted from (added to) the mean jet propagation direction.

Line 23 - .....jet occurrence "on" solar wind parameters.....

Line 30 - ...with the higher velocity and density..

We agree with the referee and will revise the manuscript accordingly.

Line 39 - ..."jets can trigger and suppress reconnection", this connection it seems contradictory, it needs to be explained

We agree with the referee that we need more explanation. We intended to say that jets can modify the magnetic field by dragging the frozen-in field lines [Hietala et al., 2018]. With the modified magnetic field they can change the shear angle between magnetospheric and magnetosheath magnetic field lines [Hietala et al., 2018]. This could trigger reconnection under conditions where we would normally wont see it (e.g. northward IMF) and vice versa (e.g. southward IMF) [see also Vuorinen et al., 2021]. We will rewrite this point in the revised manuscript.

Line 41 – I would suggest to skip ....."for a single event"....

Line 66 – ..."the central axis of this jet from evasive motion of the ambient plasma", the sentence in this place is not clear

Line 70 and elsewhere in the text – "spin resolution" instead of spin fit resolution

We agree with the referee and will revise the manuscript accordingly.

Line 95 – in the description of Fig. 2, the link to Fig. 3 is not correct

We agree with the referee that we should not include information that were not already explained.

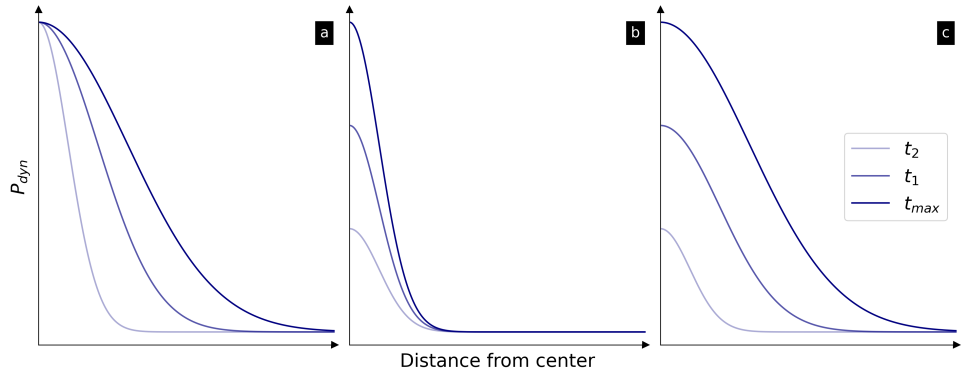

Figure 9: Hypothetical fits to dynamic pressure measurements plotted against distance from center for three different scenarios of jet shapes. In all columns fits for three different times (= different intersections of the jet) are shown. The darkest color correspond to a fit at $t_{\max}$ and lighter colors correspond to later times ($t_{\max} < t_1 < t_2$). The shown cases are described and explained in the text.

We are restructuring sections 2 and 3 of the current manuscript to improve readability.

References

Hietala, H., Phan, T. D., Angelopoulos, V., Oieroset, M., Archer, M. O., Karlsson, T., and Plaschke, F. (2018). In situ observations of a magnetosheath high-speed jet triggering magnetopause reconnection. *Geophys. Res. Lett.*, 45(4):1732–1740. doi: 10.1002/2017GL076525.

Plaschke, F. and Hietala, H. (2018). Plasma flow patterns in and around magnetosheath jets. *Ann. Geophys.*, 36(3):695–703. doi: 10.5194/angeo-36-695-2018.

Raptis, S., Karlsson, T., Vaivads, A., Lindberg, M., Johlander, A., and Trollvik, H. (2022). On magnetosheath jet kinetic structure and plasma properties. *Geophysical Research Letters*, 49(21):e2022GL100678. doi: 10.1029/2022GL100678.

Vuorinen, L., Hietala, H., Plaschke, F., and LaMoury, A. T. (2021). Magnetic field in magnetosheath jets: A statistical study of bz near the magnetopause. *Journal of Geophysical Research: Space Physics*, 126(9):e2021JA029188. e2021JA029188 2021JA029188.